https://doi.org/10.7840/kics.2025.50.5.793

Impact of Beam Split and IQ Mismatch on BER Performance of IRS-aided THz Communications

Sanjeev Sharma◆, Yeon Ho Chung°

ABSTRACT

Intelligent reflecting surfaces (IRS) and multiple-input and multiple-output (MIMO)-based design are considered for mitigating the effects of molecular absorption in terahertz (THz) systems operating at high-frequency bands. In this THz system, the phenomenon of beam splitting occurs at both the transceiver and IRS. In this paper, time-delay (TD) and delay-phase (DP) based precoding at the transmitter (Tx) and IRS are introduced to overcome the effect of beam splitting. The average bit error rate (BER) of the THz system is analyzed by considering the impact of transmitting antennas, reflecting elements, and in-phase and quadrature (IQ) mismatch for a multi-carrier system. The analysis results show that the beam splitting leads to a reduction in the BER performance by as much as 20 dB.

Key Words : Beam Split, BER Performance, IQ Mismatch, IRS-aided MIMO THz System, Time-Delay and Delay-Phase Precoding

Ⅰ. Introduction

Terahertz (THz) communication is considered a promising technology for the next-generation wireless networks due to viability of large bandwidth. THz communication can support the ultra-high data rate with ultra-massive connectivity in a wireless network for various applications such as holographic communication, immersive virtual reality, and digital twins. As compared to millimeter Wave (mmWave) (30-100 GHz) for 5G, THz band (0.1-10 THz) can support the 10 GHz or even more channel bandwidth for data transmission. However, the transmission of THz signals is significantly hindered by substantial propagation attenuation resulting from exceedingly high carrier frequencies[1].

In the THz communication, maintaining a line-of-sight (LoS) path is essential for successful data transmission. If the LoS path is blocked or severely faded, reliable communication becomes impossible in THz bands. Recently, intelligent reflecting surfaces (IRS) have been introduced to create virtual LoS paths in the network or manipulate the channel between the transmitter (Tx) and receiver (Rx) in the THz communication. Furthermore, IRS has the capability to create additional signal propagation paths, effectively resolving blockage issues through proactive manipulation of the wireless environment. Therefore, leveraging IRS in the THz communication presents an attractive prospect for the advancement of future 6G wireless systems. Similarly, massive multiple-input multiple-output (MIMO), which employs a large antenna array to produce directional beams with high array gains, offers a solution to mitigate the considerable signal attenuation inherent in THz communications. Thus, the THz massive MIMO holds

※ This work was supported by a Research Grant of Pukyong National University(2023).
◆ First Author : IIT (BHU) Varanasi, India. Department of Electronics Engineering, sanjeev.ece@iitbhu.ac.in, 정회원
° Corresponding Author : Pukyong National University, Department of Information and Communications Engineering, yhchung@pknu.ac.kr 종신회원
논문번호 : 202409-216-0-SE, Received September 23, 2024; Revised November 25, 2024; Accepted December 17, 2024

significant promise for future next-generation wireless communications. In the THz communication, a substantial number of antennas at the Tx and a considerable number of elements at the IRS are utilized to generate highly directional and energy-focused beams. This strategy aims to counteract the significant signal propagation attenuation experienced in THz communications.

In IRS-aided MIMO THz (IMT) communication, the integration of extensive bandwidth, numerous IRS elements, and massive antennas leads to significant beam splitting. As a result, the conventional phase-shifter-based hybrid precoding architecture becomes ineffective. Recently, a delay-phase (DP) precoding (frequency-dependent) architecture has been proposed to alleviate the impact of beam splitting in IMT communication [4].

Contributions: This paper investigates the bit error rate (BER) performance of the IMT communication. We compare various DP precoding techniques for the IMT communication. Our observations indicate that double beam splitting (at IRS and Tx) can significantly reduce the BER performance of IMT communication. We analyze the impact of the number of IRS elements, Tx antennas, sub-carriers, IQ mismatch, and IRS location on BER. In addition, the effect of imperfect channel state information (CSI) with and without IQ mismatch is also analyzed. The presented results suggest that the large bandwidth of THz exacerbates the beam splitting effect and degrades the BER performance significantly.

Related Works: IRS-aided MIMO THz systems are analyzed in the literature [2-4]. Researchers are focusing on BER analysis [5], sumrate [2,3,6], signal detection [7,8], beam split effect[9,10], IRS-aided design [9,10], coverage analysis[8], outage probability (OP), and channel modeling [7] in the THz communication. While beam split effects are commonly analyzed for sumrate analysis in the literature, their impact on BER analysis in IMT system design is not considered or has received less attention. A summary of works related to beam split effects is provided in Table 1.

Ⅱ. IMT System Model

The transmitter is equipped with transmit antennas, incorporating both a time-delay (TD) network and phase shifts (PS). Modulated data undergoes precoding by a digital precoder before being transmitted through the radio-frequency (RF) chains, as depicted in Fig. 1. The IRS panel comprises elements arranged horizontally and vertically. The direct LoS between Tx and Rx is obstructed due to severe fading or obstacles, with a virtual LoS established between them via the IRS. To mitigate the effect of beam splitting in the IMT communication, frequency-dependent precoding is implemented at the Tx, while DP shifting is applied at the IRS panel. Rx employs maximum likelihood signal detection and is equipped with a single antenna.

The commonly employed orthogonal frequency division multiplexing (OFDM) scheme with M sub-carriers is considered. The received downlink signal, denoted as y_m at the m-th sub-carrier ($m=1,\cdots,M$), can be expressed as

Table 1. A Summary of Representative Works on Beam Split Effect in THz System

Reference	Work	Contribution
[2, 3, 6]	Sumrate analysis	Beam split effect analysis and time-delay (TD) module design in THz
[11]	Mean square error analysis	Near field channel estimation impact in THz
[12]	Array gain analysis	Beam forming design in THz
[13]	Sumrate analysis	Hybrid beamformers design using deep learning approach in THz
[14,16]	Sumrate analysis	Multiuser precoding design using deep learning in THz
[4]	Energy efficiency and sumrate analysis	Impact of beam split effect and possible TD based solution in THz
Proposed work	BER analysis	Impact of beam split and IQ mismatch in IRS-aided massive MIMO THz

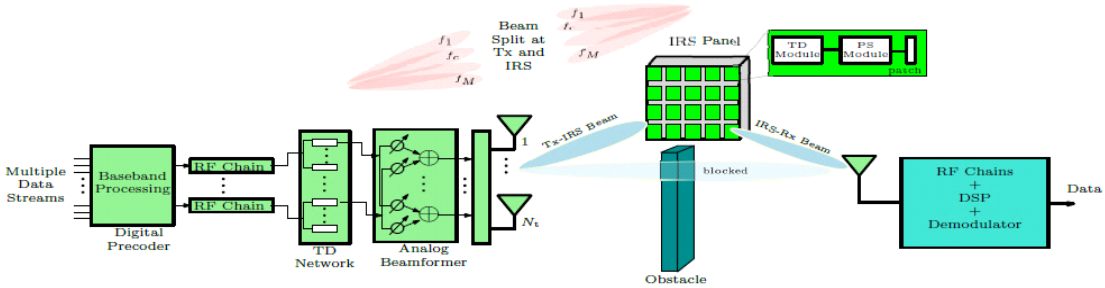

Fig. 1. An IRS-aided massive MIMO THz (IMT) communication system block diagram with DP and TD precoding.

$$y_m = \mathbf{h}_m^{\mathrm{T}} \boldsymbol{\Theta} \mathbf{G}_m \mathbf{w} x_m + n_m \in \mathbb{C}. \tag{1}$$

The expression $\mathbf{w}x_m \in \mathbb{C}^{N_t \times 1}$ signifies the transmitted signal at the Tx. Here, $x_m \in \mathbb{C}$ denotes the transmitted information symbol at the m-th sub-carrier, ensuring unit energy, i.e., $\mathrm{E}[|x_m|^2] = 1$, while $\mathbf{w} \in \mathbb{C}^{N_t \times 1}$ represents the precoding vector. Additionally, n_m represents the additive white Gaussian noise (AWGN) with zero mean and variance σ^2. The matrix $\mathbf{G}_m \in \mathbb{C}^{N \times Nt}$ represents the Tx-RIS channel response. The vector $\mathbf{h}_m^{\mathrm{T}} = [h_{m,1}, h_{m,2}, \ldots, h_{m,N}] \in \mathbb{C}^{1 \times N}$ denotes the channel from the IRS to the Rx at the m-th sub-carrier.

The response of each IRS element to the incident signal is expressed as $a_n e^{j\theta_n}$, $n = 1, 2, \ldots, N$, where θ_n is the phase and an denotes the reflection coefficient. Thus, the overall IRS panel response can be written as

$$\boldsymbol{\theta} = [a_1 e^{j\theta_1}, a_2 e^{j\theta_2}, \ldots, a_N e^{j\theta_N}]^{\mathrm{T}}. \tag{2}$$

The IRS matrix is denoted as $\boldsymbol{\Theta} = \mathrm{diag}[\boldsymbol{\theta}]$, where the expression $\mathrm{diag}[\boldsymbol{\theta}]$ represents a diagonal matrix constructed with elements selected from the vector $\boldsymbol{\theta}$.

The channel matrix $\mathbf{G}_m$ between Tx-IRS panel is

$$\mathbf{G}_m = g_1(f_m, d_1)\, e^{-j2\pi\tau_1 f_m} \mathbf{a}(f_m, \eta_1^r, \zeta_1^r)\, \mathbf{b}^{\mathrm{H}}(f_m, \phi), \tag{3}$$

where τ_1 is the path delay from Tx to IRS. $j = \sqrt{-1}$ is a complex number. The path gain $g_1(f_m, d_1) \in \mathbb{C}$ is expressed as

$$g_1(f_m, d_1) = \frac{c}{4\pi f_m d_1} e^{-\frac{1}{2}\tau_{\mathrm{abs}}(f_m) d_1}, \tag{4}$$

where c denotes the speed of light, and d_1 is the distance from the Tx to the IRS panel. $\tau_{\mathrm{abs}}(f_m)$ is the molecular absorption coefficient at the m-th sub-carrier frequency f_m. The elevation angle and the azimuth angle of the angle-of-arrival (AoA) of the RIS panel are denoted as η_1^r and ζ_1^r, respectively. The transmit angle of the Tx is denoted as ϕ. Furthermore, in the channel matrix, we assume that a LoS path exists between the Tx and the IRS panel.

The steering vector $\mathbf{a} \in \mathbb{C}^{N \times 1}$ of IRS panel having uniform planar array (UPA) is expressed as

$$\mathbf{a}(f_m, \eta, \zeta) = \frac{1}{\sqrt{N_1 N_2}} \left[1, \ldots, e^{j2\pi \frac{f_m}{c}(N_1 - 1) d \sin(\eta) \cos(\zeta)}\right]^{\mathrm{T}} \otimes \left[1, \ldots, e^{j2\pi \frac{f_m}{c}(N_2 - 1) d \sin(\eta) \cos(\zeta)}\right]^{\mathrm{T}} \tag{5}$$

The steering vector $\mathbf{b}(f_m, \phi) \in \mathbb{C}^{N_t \times 1}$ of the uniform linear array (ULA) is expressed as

$$\mathbf{b}(f_m, \phi) = \frac{1}{\sqrt{N_t}} \left[1, e^{j2\pi \frac{f_m}{c} d \sin(\phi)}, \ldots, e^{j2\pi \frac{f_m}{c}(N_t - 1) d \sin(\phi)}\right]^{\mathrm{T}}.$$

Similarly, the channel vector $\mathbf{h}_m$ between IRS and Rx is expressed as

$$\mathbf{h}_m = g_2(f_m, d_2)\, e^{-j2\pi\tau_2 f_m} \mathbf{a}(f_m, \eta_2^t, \zeta_2^t) \in \mathbb{C}^{N\times 1}, \tag{6}$$

where τ_2 is the path delay from IRS to Rx. The path gain $g_2(f_m, d_2)$ is expressed as

$$g_2(f_m, d_2) = \frac{c}{4\pi f_m d_2} e^{-\frac{1}{2}\tau_{\text{abs}}(f_m) d_2}, \tag{7}$$

where d_2 is the distance from the IRS panel to the Rx. η_2^t and ζ_2^t are the elevation angle and the azimuth angle of the angle-of-departure (AoD) at the IRS panel, respectively. These angles satisfy $\eta \in \mathbb{U}(0, \pi/2)$, $\zeta \in \mathbb{U}(-\pi, \pi)$, and $\phi \in \mathbb{U}(-\pi/2, \pi/2)$, where $\mathbb{U}[a, b]$ denotes the uniform distribution between *a* and *b*.

Ⅲ. Delay-phase Precoding at IRS

In the DP architecture, the frequency-dependent reflection coefficient of the *n*-th IRS element is characterized by $e^{j(\theta_n - 2\pi f_m \tau_n)}$, where τ_n represents the time delay. By appropriately adjusting the time delay of each element, the beams produced across various carriers can be synchronized with the desired target or physical direction. This synchronization effectively eradicates the beam split phenomenon in the IMT communication. Nonetheless, the utilization of TD modules typically entails significantly greater power consumption and hardware expenses when contrasted with systems employing solely phase shifters [2] .

To mitigate high hardware complexity and power consumption, a sub-connected architecture for IRS is preferred. Each component within the sub-array is equipped with dual-layer phase shifters and is connected to a shared TD module via a circulator [2]. Initially, the signal received at each component passes through the first-layer phase shifter, aiming to create constructive interference within the sub-array. Next, the signal is adjusted by the shared TD module. Finally, the signal passes through the second-layer phase shifter to complete the beamforming process of the IRS.

Let $Q_1 \times Q_2$ be the sub-arrays of an IRS panel, with each sub-array connected to a TD module. Each sub-array consists of $K_1 \times K_2$ elements, where $K_1 = N_1/Q_1$ and $K_2 = N_2/Q_2$. The index for elements in each sub-array is denoted as $k = (k_1, k_2)$, where $k_1 = 1, 2, \ldots, K_1$ and $k_2 = 1, 2, \ldots, K_2$. Each sub-array is identified by index $q = (q_1, q_2)$, where $q_1 = 1, 2, \ldots, Q_1$ and $q_2 = 1, 2, \ldots, Q_2$.

Channel models are expressed as [2]

$$\mathbf{G}_m = \frac{g_1(f_m, d_1)}{\sqrt{N_1 N_2}} e^{-j2\pi\tau_1 f_m} \mathbf{F}(f_m, \eta_1^r, \zeta_1^r)$$
$$\mathbf{H}_m = \frac{g_2(f_m, d_2)}{\sqrt{N_1 N_2}} e^{-j2\pi\tau_2 f_m} \mathbf{F}(f_m, \eta_2^t, \zeta_2^t), \tag{8}$$

where the steering matrix $\mathbf{F}$ is expressed as

$$\mathbf{F}_{n_1, n_2}(f_m, \eta, \zeta) = e^{\pi\zeta_m (n_1 \sin\eta\cos(\zeta) + n_2 \sin\eta\sin(\zeta))}. \tag{9}$$

Here, $n_1 = q_1 K_1 + k_1$ and $n_2 = q_2 K_2 + k_2$. Phase shift matrices ($\mathbf{\Theta}_1^q, \mathbf{\Theta}_2^q$) representing the first and second layers, time delay vector $\mathbf{p}_m$, and channel matrices ($\mathbf{G}_m^q, \mathbf{H}_m^q$) are generated for each sub-array. The received signal denoted by y_m^q, after traversing from the transmitter, first-layer, and second-layer phase shifters of the IRS panel, can be formulated as[2,10]

$$y_m^q = \text{sum}\Big(\mathbf{H}_m^q \odot \Big(\mathbf{\Theta}_2^q p_m^q \Big[\text{sum}\Big(\mathbf{\Theta}_1^q \odot \mathbf{G}_m^q x_m\Big)\Big]\Big)\Big), \tag{10}$$

where the TD vector $\mathbf{p}_m$ is

$$\mathbf{p}_m = e^{-j2\pi f_m \mathbf{t}}, \quad \mathbf{t} = [t_1, t_2, \ldots, t_q, \ldots, t_{Q_1 \times Q_2}]^{\mathrm{T}}.$$

Ⅳ. Time-Delay Precoding at the Transmitter

Suppose the Tx is partitioned into *P* sub-arrays,

each linked to a TD module. Let $t_{tx} \in \mathbb{R}$ represent the TD and $\mathbf{w}_{u,p}$ denotes the phase shift of the p-th sub-array (p = 1, ..., P) at the Tx. Consequently, the frequency-dependent transmit precoding of the Tx at the m-th sub-carrier can be described as

$$\mathrm{W}_m = \mathrm{W}_u \mathrm{p}_m^{\mathrm{tx}} = \mathrm{blkdiag}\left([\mathrm{w}_{u,1}, \ldots, \mathrm{w}_{u,P}] \right) . e^{-j2\pi f_m [t_1^{\mathrm{tx}}, t_2^{\mathrm{tx}}, \ldots, t_P^{\mathrm{tx}}]^{\mathrm{T}}} \tag{11}$$

where *blkdiag* denotes the block diagonal matrix. Here $\boldsymbol{W}_{\mathrm{u}}$ is defined as $\boldsymbol{W}_u = \left[\boldsymbol{w}_{u,1}, \boldsymbol{w}_{u,2}, \ldots, \boldsymbol{w}_{\mathrm{u,P}} \right]$. In addition, the elements of TD vector $\mathbf{p}_m^{\mathrm{tx}}$ and the phase shifting matrix adhere to

$$t_p^{\mathrm{tx}} = \frac{(p-1)(\zeta_m - 1) N_{\mathrm{t}} \sin(\phi)}{2 f_m P} \quad \text{and}$$

$$\left[\boldsymbol{w}_{u,1}^{\mathrm{T}}, \ldots, \mathbf{w}_{u,P}^{\mathrm{T}} \right]^T = \mathbf{b}(f_m, \phi) .$$

Here $\boldsymbol{b}(\,.\,)$ denotes the steering vector of the ULA.

V. Simulation Results

We analyze the average BER performance of the IMT communication system. Total system bandwidth is B Hz and sub-carriers are generated as

$$f_m = f_c + \frac{B}{M}\left(m - 1 - \frac{M-1}{2} \right) \text{ Hz} \tag{12}$$

Here, f_c denotes the carrier frequency, and in simulations, we consider f_c = 100 GHz. The molecular absorption coefficient is $\tau_{\mathrm{abs}}(f_m) = 5.157 \times 10^{-4}$ dB/m. The noise power is assumed to be $\sigma^2 = -95$ dBm. The perfect knowledge of the channel state information is assumed in simulations.

Fig. 2 illustrates the impact of beam split on BER performance at the IRS panel in the IMT system, considering average gain per sub-carrier. The optimal precoding denotes that each element has a separate DP unit, while the IRS precoding denotes only one DP module attached to a sub-array of IRS elements. The

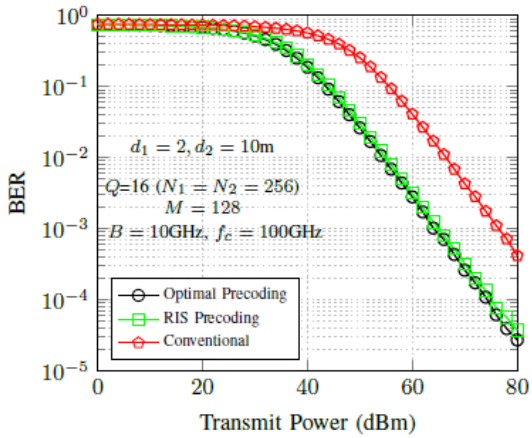

Fig. 2. Average BER performance of IMT system for N_t = 1 and TD modules=16 (N=256 × 256).

conventional IRS design uses only frequency-independent precoding by considering the center frequency only. The conventional IRS design exhibits degraded performance compared to the optimal and IRS precoding methods due to the beam split effect.

In Fig. 3, the average gain per sub-carrier of the IMT system is plotted for M= 128. It can be observed that the gain of the conventional precoding scheme reduces as we move away from the center frequency of the beam due to the beam split effect. The optimal precoding demonstrates almost a similar gain for all the sub-carriers, as observed in Fig. 3, due to the DP

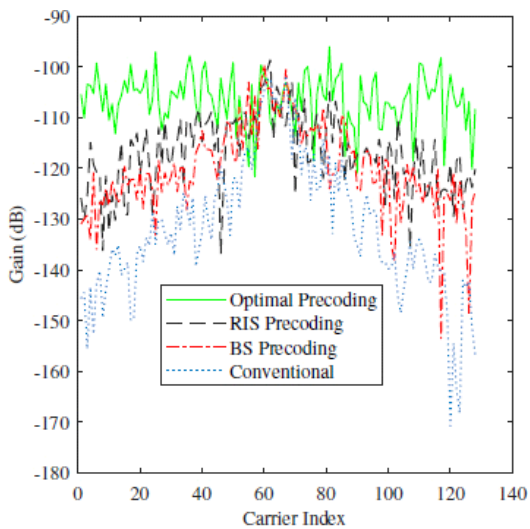

Fig. 3. Gain vs sub-carrier index plot in IMT system with N_t =256 and TD modules=16 (N=256 × 256).

precoding at the IRS and TD at the transmitter to compensate for the beam split phenomenon in the IMT. Only the IRS or the Tx exhibits improved gain compared to the conventional scheme, as the TD scheme is utilized either at the IRS or the Tx. Therefore, employing the frequency-dependent precoding at both the Tx and IRS is essential in IMT.

The impact of the number of transmit antennas on BER performance is illustrated in Fig. 4, considering the average channel gain per sub-carrier. The optimal precoding exhibits the best performance due to the reduced beam split effect in the IMT system. The

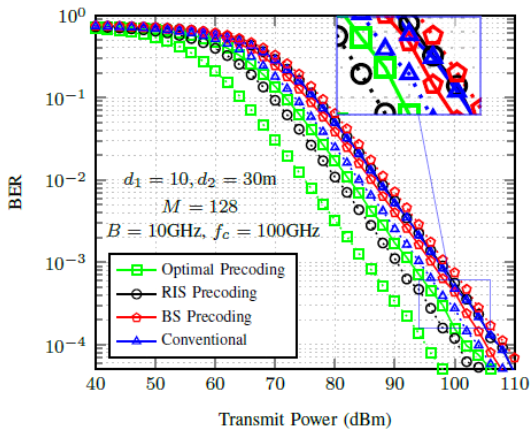

Fig. 4. Average BER performance of IMT system for Q = 8 (N = 64 × 64) with TD modules=8. Solid and dotted lines denote the performance for $N_t = 16$ and $N_t = 64$ antennas, respectively.

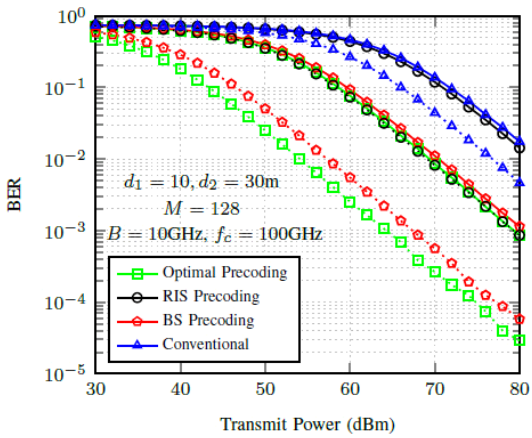

Fig. 5. Average BER performance of IMT system for $N_t = 256$ with TD modules=16. Solid and dotted lines denote the performances for Q = 16 (N = 256 × 256) and Q = 8 (N = 64 × 64), respectively.

TD-based compensation is used in the optimal, RIS, and BS precoding methods. The beam split effect is higher for $N_t = 64$, compared to $N_t = 16$. Additionally, the impact of IRS elements on BER performance is illustrated in Fig. 5, considering $N_t = 256$. The number of TD modules significantly affects the system performance, as observed in Fig. 5.

5.1 IQ Mismatch

In THz communications, the RF front-end is particularly vulnerable to IQ mismatch effects due to the extreme sensitivity of components operating at such high frequencies. IQ mismatch occurs when there is an imbalance between the inphase (I) and quadrature (Q) components, leading to signal distortions that degrade overall system performance. This imbalance, often caused by gain differences, phase errors, or non-idealities in mixers and amplifiers, results in unwanted interference between I and Q channels. Thus, at higher carrier frequencies, the IQ mismatch significantly degrades the performance of IMT systems [15]. The IQ mismatch transmitted signal is expressed as

$$x_m^{\mathrm{iq}} = \alpha_1 x_m + \alpha_2 x_m^{\star} \tag{13}$$

where $x_m^{\star}$ is the complex conjugate. IQ imbalance coefficients are such that $\alpha_1 + \alpha_2^{*} = 1$, and are given as

$$\alpha_1 = 0.5(1 + g_t e^{-j\phi_t}) \tag{14}$$

$$\alpha_2 = 0.5(1 - g_t e^{j\phi_t}) \tag{15}$$

where g_t and ϕ_t are the transmitter gain and the phase mismatch, respectively. The impact of IQ mismatch at the Tx on BER performance is analysed in Fig. 6. The BER performance deteriorates as the IQ mismatch increases, ranging from 1 dB to 10 dB, as observed in Fig. 6.

IQ mismatch at both Rx and Tx front-end: IQ mismatch at both the Tx and Rx can significantly de-

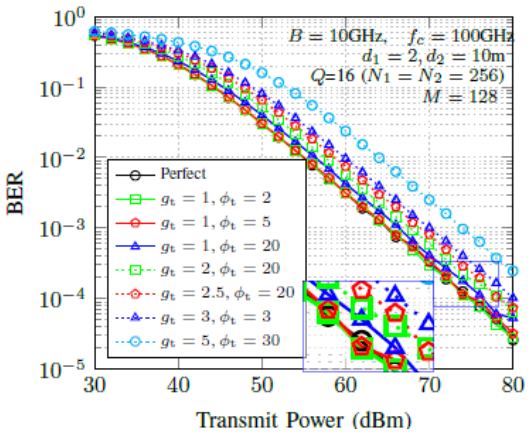

Fig. 6. Average BER performance of IMT system using optimal precoding scheme for Nt = 1 and TD modules = 16 (N = 256 × 256).

grade the performance of the IMT communication system. At the receiver, IQ mismatch affects the ability to accurately demodulate the signal, as it introduces image interference and increases interference level in the desired signal. This leads to a higher BER and reduces signal quality. IQ mismatch at Rx can be modeled as

$$y_m = \beta_1 y_m + \beta_2 y_m^* \quad , \tag{16}$$

where $\beta_1 = 0.5(1 + g_r e^{-j\phi_r})$, $\beta_2 = 0.5(1 - g_r e^{j\phi_r})$ are the same parameters as Tx IQ mismatch. The average BER performance by considering IQ mismatch

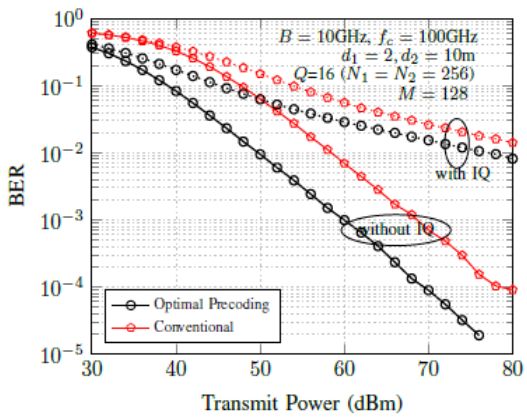

Fig. 7. Average BER performance in presence of IQ mismatch at both Tx and Rx for optimal and conventional precoding in IMT system with $g_t = 1.5$, $\phi_t = 20$ and $g_r = 1.5$, $\phi_r = 20$

at both Tx and Rx is shown in Fig. 7. BER performance degrades significantly as compared to IQ mismatch as observed in Fig. 7. Thus, it is crucial to implement compensation techniques to mitigate these impairments, especially in high-frequency applications like 6G networks.

Imperfect CSI: In massive and high-frequency MIMO systems, obtaining perfect channel state information (CSI) is challenging due to several factors. First, the large number of antennas in massive MIMO systems increases the complexity of channel estimation, requiring extensive training and feedback overhead. In high-frequency bands, such as terahertz frequencies, the channel experiences rapid fluctuations and high path loss, making real-time and accurate channel estimation difficult. Additionally, hardware impairments and signal propagation issues, like beam squint and severe attenuation, further complicate the acquisition of precise CSI. This makes achieving the perfect CSI impractical in such environments. The imperfect CSI is expressed as

$$\hat{\mathbf{h}} = \mathbf{h} + \mathbf{e} \tag{17}$$

where $\hat{\mathbf{h}}$ is the estimated channel. $\boldsymbol{e}$ denotes the estimation error and zero mean Gaussian distributed as $\mathbf{e} \sim N(0, \sigma_{\mathbf{e}}^2)$. The error plot for different variance σ_e^2 is shown in Fig. 8.

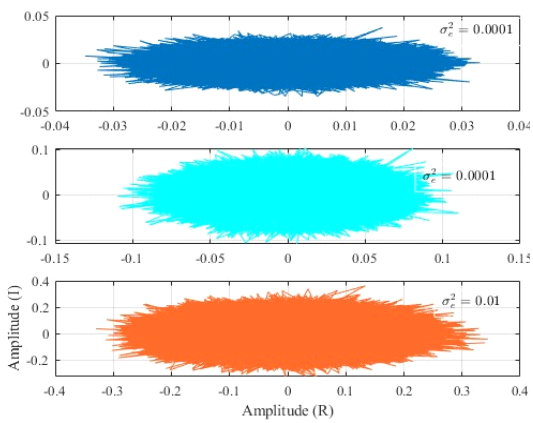

Fig. 8. Channel estimation error plot for $\sigma_e^2 = 0.01, 0.001, 0.0001$.

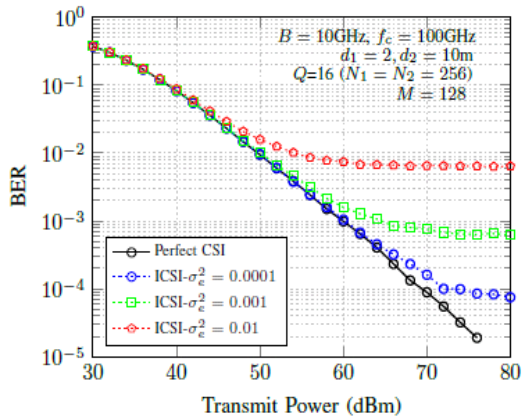

Fig. 9. Average BER plot in presence of ICSI in optimal precoded IMT system.

Average BER performance of the IMT system for imperfect CSI scenarios is shown in Fig. 9. It is observed that as error variance increases, the BER performance degrades significantly as compared to the perfect CSI scenario.

Imperfect CSI plus IQ mismatch: In an IMT system, achieving perfect CSI and mitigating IQ mismatch is particularly challenging. These factors combined make it difficult to obtain accurate CSI and correct IQ mismatches in the IMT system. The average BER performance in the presence of both imperfect CSI and IQ mismatch is shown in Fig. 10. It is observed that the BER remains very high and does not reduce as SNR increases when both the transmitter and receiver are affected by IQ mismatch with imperfect CSI. Furthermore, the imperfect CSI and IQ mismatch cause the BER to saturate, resulting in an error floor in the high SNR region, as observed in Fig. 10.

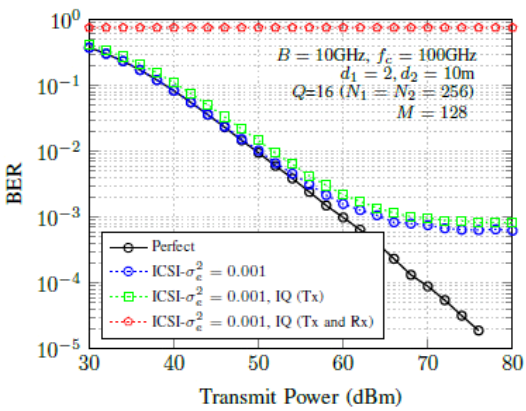

Fig. 10. Average BER plot in the presence of ICSI and IQ mismatch in optimal precoded IMT system with σ_e^2=0.01, g_t=1.5, ϕ_t=20 and g_r=1.5, ϕ_r=20.

Ⅵ. Conclusions

We have examined the BER performance within the IMT communication by considering the implications of beam splitting in the THz communication, and compared various TD precoding methods in the IMT communication. We have analyzed the effects of factors, such as the number of IRS elements, Tx antennas, and IQ mismatch, on BER. Our analysis highlights that the wide bandwidth of THz exacerbates the beam splitting effect, leading to degradation in BER performance. It is also demonstrated that the application of the DP precoding can effectively mitigate the beam splitting challenge within the IMT communication. Furthermore, the effect of imperfect CSI and IQ mismatch is highlighted on the BER performance in the IMT system.

References

[1] S. Sharma, K. Deka, and A. Mishra, "Reconfigurable intelligent surfaces aided terahertz communication for 6G: Challenges and potential solutions," *Wireless Pers. Commun.*, pp. 1-15, 2024.

[2] R. Su, L. Dai, and D. W. K. Ng, "Wideband precoding for RIS-aided THz communications," *IEEE Trans. Commun.*, vol. 71, no. 6, pp. 3592-3604, 2023.

[3] J. Gao, C. Zhong, G. Y. Li, J. B. Soriaga, and A. Behboodi, "Spatially sparse precoding in wideband hybrid terahertz massive MIMO systems," *IEEE Trans. Wireless Commun.*, 2023.

[4] J. Tan and L. Dai, "THz precoding for 6G: Challenges, solutions, and opportunities," *IEEE Wireless Commun.*, vol. 30, no. 4, pp. 132-138, 2022.

[5] V. Sharma, S. Sharma, and V. Bhatia,

"Performance analysis of intelligent reflecting surface assisted MIMO terahertz system," in *2022 IEEE Int. Conf. ANTS*, pp. 1-5, 2022.

[6] S. Kim, J. Park, J. Moon, and B. Shim, "Fast and accurate terahertz beam management via frequency-dependent beamforming," *IEEE Trans. Wireless Commun.*, 2023.

[7] H. Du, J. Zhang, K. Guan, D. Niyato, H. Jiao, Z. Wang, and T. Kürner, "Performance and optimization of reconfigurable intelligent surface aided THz communications," *IEEE Trans. Commun.*, vol. 70, no. 5, pp. 3575-3593, 2022.

[8] M. H. Kumar, S. Sharma, K. Deka, and M. K. Sharma, "RIS-assisted user pairing OMA system for THz communications," in *2023 NCC IEEE*, pp. 1-6, 2023.

[9] Q. Xue, C. Ji, S. Ma, J. Guo, Y. Xu, Q. Chen, and W. Zhang, "A survey of beam management for mmwave and THz communications towards 6G," *IEEE Commun. Surv. & Tuts.*, 2024.

[10] G. Sun, W. Yan, W. Hao, C. Huang, and C. Yuen, "Beamforming design for the distributed RISs-aided THz communications with double-layer true time delays," *IEEE Trans. Veh. Technol.*, 2023.

[11] S. Tang, Z. Dong, W. Zhou, D. Cai, E. Zhou, and P. Lan, "Beam splitting sensing for terahertz near-field channel estimation," in *2023 3rd Int. Conf. ICC, IEEE*, pp. 141-146, 2023.

[12] Y. Jiang, Z. Zhou, X. Li, and Y. Gong, "Beamforming design for RIS-aided THz wideband communication systems," in *2023 IEEE 24th Int. Wkshp. SPAWC*, pp. 296-300, 2023.

[13] A. M. Elbir, K. V. Mishra, and S. Chatzinotas, "Terahertz-band joint ultra-massive MIMO radar-communications: Model-based and model-free hybrid beamforming," *IEEE J. Sel. Topics in Signal Process.*, vol. 15, no. 6, pp. 1468-1483, 2021.

[14] Z. Liu, H. Ke, Y. Zhang, X. Zhao, Y. Liu, and M. Jin, "A deep learning-based hybrid precoding with attention mechanism for THz massive MUMIMO systems," in *ICC 2023-IEEE Int. Conf. Commun.*, pp. 5639-5644, 2023.

[15] A. Singh, S. Sharma, K. Deka, and V. Bhatia, "Deep learning-assisted OFDM detection with hardware impairments," *J. Commun. and Inf. Netw.*, vol. 8, no. 4, pp. 378-388, 2023.

[16] C. Yun and K. Choi, "Hybrid beamforming in Sub-THz LoS MIMO systems," *J. KICS*, vol. 48, no. 5, pp. 543-548, May 2023.

Sanjeev Sharma

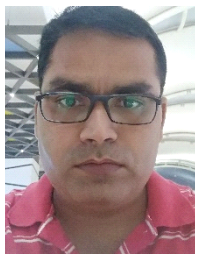

He received the M. Tech. and PhD degrees from Indian Institute of Technology Guwahati, and Indian Institute of Technology Indore in 2010 and 2018, respectively, all in Electrical Engineering. He worked in the Department of Electrical and Computer Systems Engineering at Monash University, Melbourne, Australia, as a Postdoctoral Fellow. Currently, he is working as an Assistant Professor at Electronics Engineering, IIT (BHU) Varanasi. His research interests lie in signal processing for wireless communications and networking, mathematical modelling, simulation, design, and analysis of wireless systems.

Yeon Ho Chung

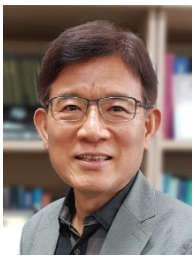

He is a Professor of the Department of Information and Communications Engineering at Pukyong National University in Busan, Korea. He earned an MSc from Imperial College London, UK, in 1992 and a Ph.D. from the University of Liverpool, UK, in 1996. He served as a visiting professor at Pennsylvania State University in University Park, US, and Chiba University in Japan. In 2017, he was a foreign expert for the GIAN program of the Government of India. He delivered keynote speeches at IFIP WMNC 2018, CSNDSP 2020, ICCWC 2021, and WASOWC 2022. He is the Editor-in-Chief of the International Journal of Sensors, Wireless Communications, and Control, published by Bentham Science. He is an associate editor of IEEE Access. Additionally, he is the Vice President of the Korean Institute of Communications and Information Sciences (KICS). He co-founded and served as the General Chair for ICMIC 2022 and ICMIC 2023 in Jeju, Korea. In 2014, he received the Top Paper Award from Transactions on Emerging Telecommunications Technologies (ETT), published by Wiley, and the Best Paper Awards from the ICGHIT and ICUFN in 2018 and 2019, respectively. He was awarded the Busan Science and Technology Award in 2020 for outstanding research achievements. His research interests include light-based wireless communications for 6G, short-range optical camera communications, outdoor and indoor optical scattering communications, and high-speed, high-capacity orbital angular momentum wireless communications for 6G.